IEEE Access
Multidisciplinary ⋮ Rapid Review ⋮ Open Access Journal

Received 13 December 2023, accepted 13 January 2024, date of publication 17 January 2024, date of current version 30 January 2024.

Digital Object Identifier 10.1109/ACCESS.2024.3355197

RESEARCH ARTICLE

Single Layer Multi-Band Transmissive Type Linear to Circular Polarization Converter With Wide Angular Stability for C-, X-, and Ku-Band Applications

HAMED SHIRZAD, CHANGIZ GHOBADI, JAVAD NOURINIA, (Senior Member, IEEE), MAJID SHOKRI, (Graduate Student Member, IEEE), AND MOHSEN KARAMIRAD

Department of Electrical Engineering, Urmia University, Urmia 57561-51818, Iran

Corresponding author: Changiz Ghobadi (ch.ghobadi@urmia.ac.ir)

ABSTRACT This paper presents a linear-to-circular polarization converter (LCPC) used for multi-band functionality. The LCPC surface features symmetrically printed copper strips on a single-layer substrate and is surrounded by a square substrate integrated waveguide (SIW) cavity arranged periodically in two dimensions. The study successfully utilizes the LCPC surface to achieve a desirable axial ratio (AR) band width (BW) below 3 dB in multiple frequency ranges, specifically: 1) 4.51-4.80 GHz, 2) 6.51-6.80 GHz, 3) 9.01-9.20 GHz, 4) 10.90-12.40 GHz, and 5) 17.05-17.49 GHz. The LCPC induces a change in polarization as the wave propagates through it. In the first (f_{31}) and fourth (f_{34}) frequency bands, the initially linearly polarized (LP) wave transforms into a left-hand circularly polarized (LHCP) wave. Conversely, in the second (f_{32}), third (f_{33}), and fifth (f_{35}) frequency bands, the wave converts into a right-hand circularly polarized (RHCP) wave. Measurement results indicate that the LCPC provides circularly polarized (CP) wave bandwidths of 12.72%, 4.8%, 2.4%, 11.39%, and 3.15% across frequency ranges of 3.9 - 4.43 GHz, 6.21- 6.52 GHz, 8.9-9.08 GHz, 10.51-11.78 GHz, and 16.85-17.39 GHz, respectively. This characteristic renders the LCPC suitable for utilization in the C (4-8 GHz), X (8-12 GHz), and Ku (12-18 GHz) frequency bands.

INDEX TERMS Circularly polarized, multi-band, polarization converter, substrate integrated waveguide.

I. INTRODUCTION

In recent years, extensive research has been conducted on the utilization of circularly polarized (CP) electromagnetic (EM) waves [1]. It is worth noting that CP waves exhibit greater immunity to different disruptive factors, such as fading through multiple paths and polarization mismatches, compared to linearly polarized (LP) waves. Hence, EM waves demonstrating circular polarization characteristics are preferred in practical applications [2], [3]. Several techniques have been proposed to design a CP antenna, including the implementation of fractal geometries as the antenna structure [4], merging two LP antennas with a 90° phase difference in their feeding network [5], employing a helical and rectangular slot in the radiation patch [6], utilizing a sequentially rotated series feeding network [7], leveraging a Wilkinson-type power divider [8], designing a four-way feeding network [9], and employing an aperture-coupled method [10]. Achieving circular polarization requires the excitation of two waves with identical amplitudes and a phase difference of 90°. However, the aforementioned methods necessitate a precise configuration of the feeding system and a complex slot arrangement on the radiator, which complicates the development of CP antennas. Planar arrays offer a promising avenue for achieving this characteristic, with a linear-to-circular polarization converter (LCPC) based on frequency selective surface (FSS)

The associate editor coordinating the review of this manuscript and approving it for publication was Shah Nawaz Burokur.

technology providing a viable solution to the challenges associated with CP antennas. According to [11], FSS techniques enable frequency filtering by selectively allowing desired frequency bands to pass through while rejecting out-of-band frequencies. In this study, multiple applications of FSS were identified, such as gain enhancement, beam shaping, minimizing the radar cross-section of antennas [12], [13], and LCPC design [14], [15], [16], [17], [18], [19], [20], [21], [22], [23], [24], [25], [26], [27], [28], [29], [30], [31], [32]. Surface-based LCPCs can be classified into two primary categories: reflective [14], [15], [16] and transmissive [18], [19], [20], [21], [22], [23], [24], [25], [26], [27], [28], [29], [30], [31], [32]. The reflective-type LCPCs based on FSS and anisotropic impedance surfaces enable the conversion from linear to circular polarization, as described in [14], [15], [16]. Although reflective-type converters with the ability to convert linear to circular polarization in multi-bands have also been introduced [16], it should be noted that in comparison to the reflective-type converter, transmissive converters minimize blockage loss and offer a more condensed system by allowing the radiating device to be placed closer to the converter than reflective converters [17]. Transmission-type LCPCs are typically constructed with periodic arrangements that transmit two LP waves with equal amplitude components and a 90° phase difference. Configurations using conventional meander lines, loop structures, and multi-layer arrangements have been reported [18], [19], [20], [21], [22]. The development of double-band transmissive-type LCPCs is described in [23], [24], [25], [26], [27], [28], [29], [30], [31], [32]. These include designs utilizing split loop structures [23], [24], planar-dipole and quasi-two-wire transmissive line couplers [25], multi-layer architectures with resonators and patches [26], three-layer dual-band LCPCs [27], [28], K-band compatible asymmetric converters [30], and multi-layer dual-band LCPCs [31], [32]. Despite the significant progress achieved in dual-band transmissive-type polarization converters discussed in previous studies [23], [24], [25], [26], [27], [28], [29], [30], [31], [32], the development of multi-band transmissive-type polarization converters remains a major challenge. The demand for such converters has been widespread in modern communication systems of the latest generations. One key challenge in developing these converters is the simultaneous management of two fundamental variables: the transmissive coefficient (TC) magnitude and the phase discrepancy. A novel design procedure involving the optimization of geometric parameters of a meta sheet was employed to create a triple-band LCPC [33]. Furthermore, [34] introduces a triple-band transmissive LCPC with three operational frequency bands, featuring multiple rings and copper patches in its structure.

This study presents a multi-band transmissive LCPC of a novel design methodology founded upon optimizing geometric parameters. To show the design concepts of the multi-band LCPC, a prototype of a 16 × 16 array of its unit cell (UC) has been fabricated. The constructed converter's transmissive properties are evaluated by positioning it between two standard horn antennas. This study introduces a highly practical five-band LCPC that boasts several remarkable features. Firstly, it stands out as one of the earliest designs of its kind. Secondly, unlike other LCPCs that operate on multiple bands and require multiple layers, this LCPC is configured on a single-layer substrate, resulting in a simple, cost-effective, and easy fabrication process. Moreover, the proposed structure consistently performs well across a wide range of angles. Lastly, the circular polarization characteristics of the first and fourth bands differ from the second, third, and fifth bands, making it an exceptional option for situations that require polarization diversity.

II. THEORETICAL INVESTIGATION AND BASICS OF LCPC

To elucidate the process of polarization conversion, we will first explore the transmission of a plane EM wave through a LCPC. Subsequently, we will investigate the mechanisms underlying the alteration of the wave. The relationship between the complex magnitudes of the incident (E^i) and transmitted (E^t) fields can be described by the T-matrix, as stated in [35]:

$$\begin{bmatrix} E_x^t \\ E_y^t \end{bmatrix} = T \begin{bmatrix} E_x^i \\ E_y^i \end{bmatrix} = \begin{bmatrix} t_{xx} & t_{xy} \\ t_{yx} & t_{yy} \end{bmatrix} \begin{bmatrix} E_x^i \\ E_y^i \end{bmatrix} \tag{1}$$

In this study, the following notation is adopted: $t_{ij}; i = j$ represents the co-polarized TC and $t_{ij}; i \neq j$ denotes the cross-polarized TC. Generally, the propagated CP wave can be considered as the superposition of two mutually perpendicular waves with equal amplitudes. Therefore:

$$\vec{E^t} = \vec{E_x^t} + \vec{E_y^t} = E_o^t \left(T_x \boldsymbol{x} + T_y \boldsymbol{y}\right) e^{-jkz} \tag{2}$$

Here, E_0^t corresponds to the amplitudes of the transmitted CP wave. The matrix below has been considered to represent the linear base transmittance.

$$\begin{bmatrix} T_x \\ T_y \end{bmatrix} = \begin{bmatrix} |T_x| e^{j\varphi} \\ |T_y| e^{j\varphi} \end{bmatrix} \tag{3}$$

When an LP wave is transmitted through an LCPC, it results in the generation of a CP wave, characterized by two orthogonal electric field components that have a phase difference. The presence of both $|T_x| = |T_y|$ and $\Delta\varphi = \pm 90°$ leads to the propagation of the CP wave. This principle must be adhered to across all multiple frequency bands in the LCPC. The term "TC" is conventionally defined or referenced as:

$$T.C = \left(E^t / E^i\right) \tag{4}$$

The transmitted wave of CP may be defined as indicated in [36]:

$$\begin{bmatrix} E_{RHCP}^t \\ E_{LHCP}^t \end{bmatrix} = \begin{bmatrix} E_x^t + jE_y^t \\ E_x^t - jE_y^t \end{bmatrix} = (T.C)_{circular} \begin{bmatrix} E_x^i \\ E_y^i \end{bmatrix} \tag{5}$$

$$\begin{aligned} (T.C)_{circular} &= \begin{pmatrix} T_{RHCPx} & T_{RHCPy} \\ T_{LHCPx} & T_{LHCPy} \end{pmatrix} \\ &= \frac{1}{\sqrt{2}} \begin{pmatrix} T_{xx} + jT_{yy} & T_{xy} + jT_{yy} \\ T_{xx} - jT_{yx} & T_{xy} - jT_{yy} \end{pmatrix} \end{aligned} \tag{6}$$

In (6), the parameter "$1/\sqrt{2}$" is employed as a normalization factor for power. The equation demonstrates the capability of the proposed LCPC to convert incident LP waves into transmitted CP waves. The LCPC under investigation exhibits negligible cross coefficients ($T_{xy} \approx T_{yx} \approx 0$). Consequently, using (5) and (6), we obtain:

$$E^t_{RHCP} = \frac{1}{\sqrt{2}}\left[(T_{xx})\,E^i_x + (jT_{yy})\,E^i_y\right] \tag{7}$$

$$E^t_{LHCP} = \frac{1}{\sqrt{2}}\left[(T_{xx})\,E^i_x - (jT_{yy})\,E^i_y\right] \tag{8}$$

III. PRESENTATION OF THE PROPOSED UNIT CELL

The proposed LCPC UC utilizes Rogers 4003 as the substrate material, characterized by a relative permittivity of 4.3 and a loss tangent of 0.025. The designed UC structure, as depicted in Fig.1, serves as the focal point for the current study.

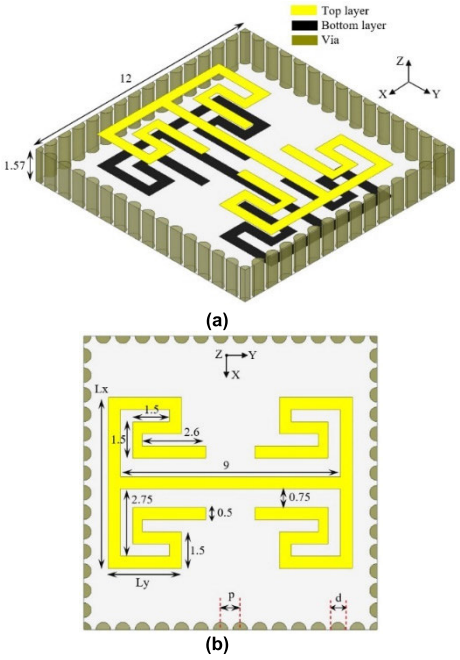

FIGURE 1. Schematic of the proposed multi-band UC for the LCPC (a) perspective view (b) top view (all dimensions are in mm).

The converter design incorporates several objectives. Firstly, the LCPC is designed to withstand significant angular variations of incident waves. Achieving this necessitates that the dimensions of the metal element, embedded on the substrate, remain below half the wavelength of the center frequency within the lowest operating band. Consequently, the geometric structure selected for the UC is a square cube with dimensions of 12.00 mm × 12.00 mm × 1.57 mm, surrounded by copper-filled vias. The arrangement of vias in Fig. 1 is classified as a substrate integrated waveguide (SIW) cavity. These vias, spaced at a distance of p = 0.8 mm from each other, possess a diameter of d = 0.6 mm. Detailed dimensions of the proposed LCPC UC are presented in Fig.1 (b), where all metal strips are fabricated using 35 μm thick copper. The second objective focuses on achieving broadband performance for the converter, with resonance elements employed to facilitate this goal. To this end, an inductive metal strip with a length of 9 mm is positioned at the center of the converter. Additionally, in order to achieve circular polarization, a phase difference of 90° must be realized between the incident LP waves. Thus, apart from the aforementioned central strip, metal strips perpendicular to each other are incorporated into the design pattern. It should be noted that the pattern must possess rotational asymmetry to induce rotation of the current distribution vector (CDV) on the plate. The metal strips, resembling inductors and capacitors, can be adjusted in dimensions to manage the band width (BW) of the converter. Notably, cross shapes have also been considered as potential patterns for LCPC UC design, as referenced in [36], [37]. For efficient coupling of radiation waves into the cavity, y-direction and perpendicular curves have been utilized to transmit the field from the surface. Improvement of incident wave propagation is achieved through symmetrical copper curves positioned on both the top and bottom surfaces of the substrate. Consequently, a single-layer structure is employed to accommodate the desired phase difference, freedom in broadband circular polarization design, and eliminate the need for multi-layer designs and structures. Extra elements perpendicular to the main strip (in both x and y-directions) are integrated into the single-layer substrate. The suggested LCPC's response to LP waves is evaluated utilizing the Microwave Studio CST software. Periodic boundary conditions are imposed along the principal axes (x- and y-axes) to simulate the infinite dimensions of the configuration. Effective refinement of the LCPC's performance is accomplished through appropriate adjustment of geometric parameters. The axial ratio (AR) measure is employed to characterize wave polarization properties, considering the TCs and the phase discrepancy between them. The AR criterion is defined according to [36]:

$$\mathbf{AR} = \mathbf{10}\log_{10}(\mathcal{U}/\mathcal{V}) \tag{9}$$

where $\mathcal{U}$ and $\mathcal{V}$ are:

$$\mathcal{U} = \left(\mathbf{T_{xx}}\cos\tau + \mathbf{T_{yy}}\cos\Delta\varphi\sin\tau\right)^2 + \left(T^2_{yy}sin^2\Delta\varphi sin^2\tau\right) \tag{10}$$

$$\mathcal{V} = \left(T_{xx}\sin\tau + T_{yy}\cos\Delta\varphi\cos\tau\right)^2 - \left(T^2_{yy}sin^2\Delta\varphi cos^2\tau\right) \tag{11}$$

where τ is:

$$\tau = \mathbf{1}\Big/\mathbf{2}\tan^{-1}\left(\left(2\mathbf{T}_{xx}T_{yy}\cos\Delta\varphi\right)\Big/\left(\mathbf{T}^2_{xx} - \mathbf{T}^2_{yy}\right)\right) \tag{12}$$

IV. DETAILS OF MULTI-BAND LCPC UC DESIGN

To evaluate and demonstrate the simulated results of the LCPC, a comprehensive simulation is conducted using the CST software program. The LCPC UC is excited by a plane wave incident at an angle of $\varphi = 45^o$ with respect to the cell. The proposed design methodology for the LCPC follows a three-step process that involves modifications to

the UC structure. These steps, along with their corresponding co-polarized TCs and phase differences, are illustrated in Fig. 2. Ensuring equal and perpendicular amplitudes of co-polarized TCs (txx & tyy) is crucial for the proper functioning of the LCPC. This requirement has been carefully examined and investigated in the three phases of the converter design. In the first design step (Fig. 2(a)), circular polarization conditions are achieved only in three frequency bands centered at $f_{11} = 7.9, f_{12} = 11.6$, and $f_{13} = 15.4$ GHz, as shown in Fig. 2(d). To clarify, when we refer to "f_{nm}" we are specifying the central operating frequency of the nth development phase within the mth operating band.

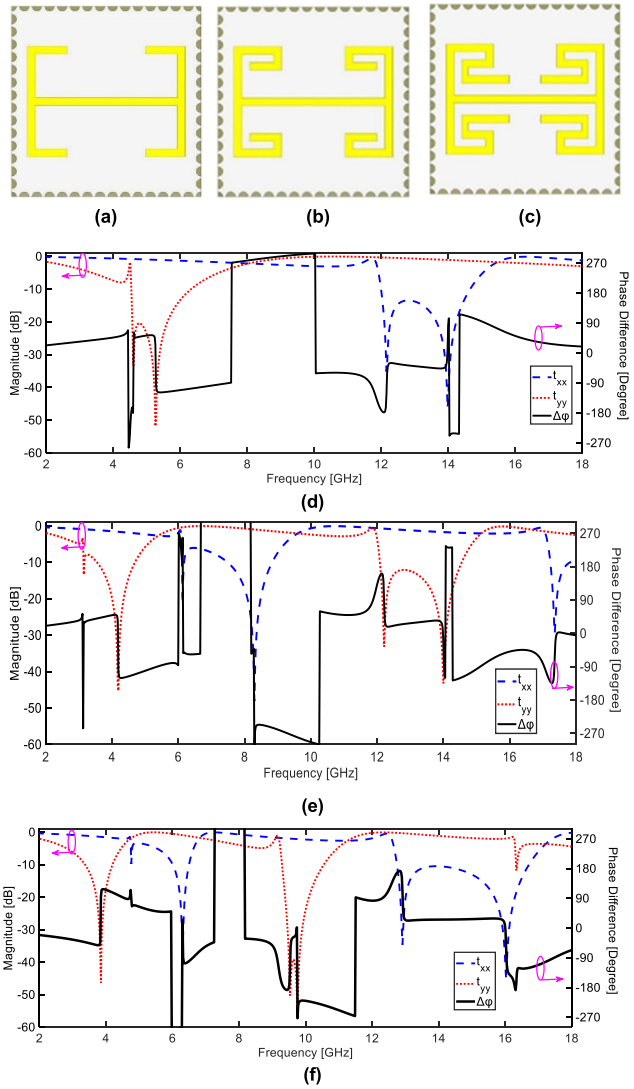

FIGURE 2. Three-step evolution of multi-band LCPC (a) first structure, (b) second structure, (c) last structure, and co-polarized TCs (magnitude and phase difference) responses related to (d) first structure, (e) second structure, and (f) last structure.

The amplitude of co-polarized TCs for the first band is approximately equal and exceeds −1 dB within the frequency range of 7.7 GHz < B.W$_1$ < 8.5 GHz. The phase difference of co-polarized TCs falls within the range of $-100° < \Delta\varphi < -89°$ within the frequency range of 6.71 GHz < B.W$_{21}$ < 7.5 GHz. In the frequency range of 7.53 GHz < B.W$_{22}$ < 8.22 GHz, the phase difference between txx and tyy alters between $271° < \Delta\varphi < 280°$. The intersection of the above-mentioned bandwidths (B.W$_1$ ∩ (B.W$_2$ = (B.W$_{21}$ ∪ B.W$_{22}$)) indicates left-hand circularly polarized (LHCP) within the frequency range of 7.7 GHz < B.W$_3$ < 8.22 GHz. Here, B.W$_{1k}$, B.W$_{2k}$, and B.W$_3$ refer to specific frequency ranges. B.W$_{1k}$ represents the range where $T_{xx} \approx T_{yy} \geq -1dB$ is satisfied. B.W$_{2k}$ represents the range where $\Delta\varphi \approx \pm 180^o \pm 90^o$ is fulfilled. Finally, B.W$_3$ represents the frequency range of intersection where the CP wave is achieved. Similar explanations apply to the other two frequency bands centered at $f_{12} = 11.6$ and $f_{13} = 15.4$ GHz. In the second design step, the inclusion of a metallic L-shaped strip (Fig.2(b)) enables circular polarization in four frequency bands with central frequencies of $f_{2m} = 5.6$, 9.55, 15.14, and 16.9 GHz, as observed in Fig. 2(e). Lastly, in the third design step, the introduction of a Γ-shaped metal line (Fig. 2(c)) extends the converter's capability to convert linear to circular polarization in five frequency bands centered at $f_{3m} = 4.65$, 6.65, 9.10, 11.65, and 17.33 GHz (Fig.2(f)). Detailed information regarding this study is provided in Table 1. The AR criterion is employed to validate the presence of transmitted CP waves. The simulated AR, along with the phase difference, is presented in Fig. 3. In the frequency spectrum of operation for the proposed LCPC, both AR ≤ 3 dB and phase differences within the range of $\Delta\varphi \approx \pm 180^o \pm 90^o$ for co-polarized TCs are simultaneously achieved. Consequently, after passing through the LCPC, LP waves in five frequency bands are converted to right-hand circularly polarized (RHCP) or LHCP waves. The RHCP characteristic is observed as the output of the LCPC in the first (f_{31}) and fourth (f_{34}) frequency bands. Conversely, the LHCP characteristic is observed as the LCPC output in the second (f_{32}), third (f_{33}), and fifth (f_{35}) frequency bands.

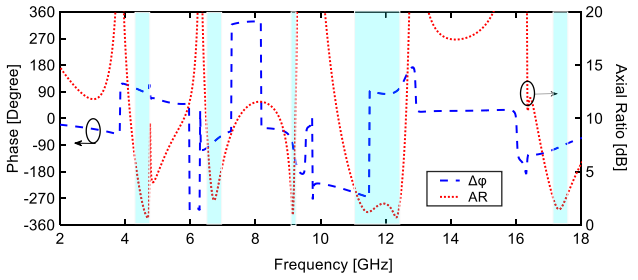

FIGURE 3. Simulated TC Phase difference and AR of the proposed multi-band LCPC.

V. CURRENT DISTRIBUTION ANALYSIS

Figs 4(a-d) illustrate the resulting CDVs at $f_{31} = 4.65$ GHz. As depicted in Fig. 4(a), at t = 0, the simulated CDV aligns parallel to the x-axis. Moving to Fig. 4(b), at t = T/4, the CDV exhibits an angle of approximately −90° with respect to the x-axis. Similarly, in Fig. 4(c), at t = T/2, the CDV aligns

TABLE 1. Details of the multi-band LCPC design steps.

Steps	B. W_1 (GHz) for Txx ≈ Tyy	B. W_2 (GHz) for $\Delta\varphi \approx \pm 180^o \pm 90^o$	B.W_3 = B. W_1 ∩ B. W_2	Center Freq (GHz) f_{nm}	Polarization
# 1	1 < B.W_1 <1.64	B.W_2 = ∅	B.W_3 = ∅	---	NO CP
	7.7< B.W_1 < 8.5	6.71 < B.W_2 < 8.22	7.7< B.W_3 <8.22	f_{11} =7.9	LHCP
	11.5< B.W_1 <11.8	11.5< B.W_2 < 11.7	11.5< B.W_3 <11.7	f_{12} =11.6	LHCP
	15.3< B.W_1 < 15.7	14.5< B.W_2 <15.55	15.3< B.W_3 <15.5	f_{13} =15.4	RHCP
# 2	1< B.W_1 <1.64	B.W_2 = ∅	B.W_3 = ∅	---	NO CP
	5.23< B.W_1 <5.98	5 < B.W_2 < 6.01	5.23 < B.W_3 < 5.98	f_{21} =5.6	LHCP
	9.45 < B.W_1 < 9.8	8.9 < B.W_2 < 9.65	9.45 < B.W_3 < 9.65	f_{22} =9.55	RHCP
	15.02 < B.W_1 < 15.30	14.92 < B.W_2 < 15.26	15.02 < B.W_3 < 15.26	f_{23} =15.14	LHCP
	16.37 < B.W_1 < 17.09	16.85 < B.W_2 < 17.11	16.85 < B.W_3 < 17.09	f_{24} =16.9	LHCP
	B.W_1 = ∅	18.99 < B.W_2 < 19.24	B.W_3 = ∅	---	NO CP
# 3	1 < B.W_1 < 1.62	B.W_2 = ∅	B.W_3 = ∅	---	NO CP
	4.51 < B.W_1 < 4.80	4.42 < B.W_2 < 4.85	4.51< B.W_3 < 4.80	f_{31} =4.65	RHCP
	6.51 < B.W_1 < 6.80	6.49 < B.W_2 < 6.80	6.51< B.W_3 < 6.80	f_{32} =6.65	LHCP
	8.90 < B.W_1 < 9.51	9.01 < B.W_2 < 9.20	9.01 < B.W_3 < 9.20	f_{33} =9.10	LHCP
	10.90 < B.W_1 < 12.55	10.82 < B.W_2 < 12.40	10.90< B.W_3 < 12.40	f_{34} =11.65	RHCP
	17.05 < B.W_1 < 17.49	17.01 < B. W_2 < 17. 62	17.05 < B.W_3 < 17.49	f_{35} =17.33	LHCP

∅ is the null sign.

in the same direction as the -*x*-axis. Lastly, Fig. 4(d) shows that at t = 3T/4, the CDV aligns in the same direction as the *y*-axis. Notably, at each division of T/4, the CDV undergoes an approximate 90° clockwise rotation. Consequently, the transmitted wave at f_{31} = 4.65 GHz manifests as RHCP. A comparable investigation is conducted for f_{32} = 6.65 GHz. As depicted in Figs 4(e-h), the CDV is monitored throughout an entire period (=T) with intervals of T/4. This analysis reveals a counter-clockwise rotation of the CDV. Thus, the output wave from the converter at f_{32} gives rise to LHCP radiation. Similarly, the CDV is simulated over a period with intervals of T/4 at frequencies of f_{33} = 9.10 GHz, f_{34} = 11.65 GHz, and f_{35} = 17.33 GHz. Figure 4 illustrates that the output waves of the LCPC correspond to LHCP, RHCP, and LHCP at frequencies of f_{33}, f_{34}, and f_{35}, respectively.

VI. PARAMETRIC STUDY

In order to investigate the impact of different metallic parameters on the co-polarized TCs (txx and tyy) of the proposed LCPC, an analysis on key parameters (*Lx* and *Ly*) was conducted while keeping other parameters constant. Figure 5 illustrates the findings regarding the influence of the *Lx*-parameter on the magnitude of the txx coefficient within the operating bands. It can be observed that increasing the value of the *Lx*-parameter leads to a decrease in the magnitude of the txx coefficient. Additionally, a shift in the resonant frequency towards lower frequencies is evident. Subsequently, the next analysis focuses on the effects of the *Ly*-parameter on the txx coefficients.

Figure 6 reveals a contrasting trend compared to the observations presented in the previous figure. Specifically, an increase in the *Ly*-parameter value correlates with an amplified magnitude of the *x*-polarized transmitted wave (txx), accompanied by a shift in the resonant frequency towards higher frequencies. In order to comprehensively investigate the characteristics of the *y*-polarized transmitted wave (tyy), variations in the *Lx* and *Ly*-parameters were investigated. The outcomes of these investigations are visualized in Fig. 7 and Fig. 8. The observed changes in the *y*-polarized transmitted wave (tyy) and the resonant frequencies, resulting from the increase in the *Lx* and *Ly*-parameters, align consistently with the patterns depicted in Fig.5 and Fig.6. After careful analysis of the provided explanations and in pursuit of optimal alignment, as indicated in Table 1, the values

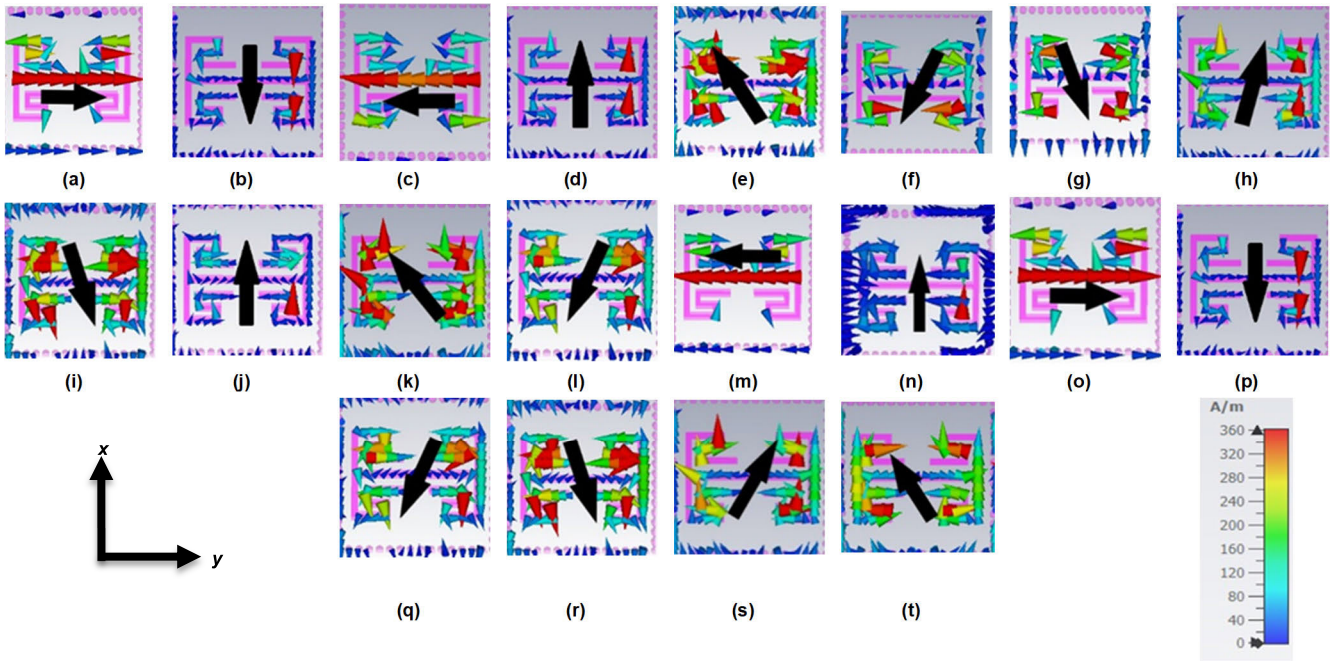

FIGURE 4. Surface CDV of the proposed LCPC at (a) f_{31}, t = 0, (b) f_{31}, t = T/4 (c) f_{31}, t = T/2 (d) f_{31}, t = 3T/4 (e) f_{32}, t = 0 (f) f_{32}, t = T/4 (g) f_{32}, t = T/2 (h) f_{32}, t = 3T/4, (i) f_{33}, t = 0 (j) f_{33}, t = T/4 (k) f_{33}, t = T/2 (l) f_{33}, t = 3T/4, (m) f_{34}, t = 0 (n) f_{34}, t = T/4 (o) f_{34}, t = T/2 (p) f_{34}, t =3T/4, (q) f_{35}, t = 0 (r) f_{35}, t = T/4 (s) f_{35}, t = T/2 (t) f_{35}, t = 3T/4.

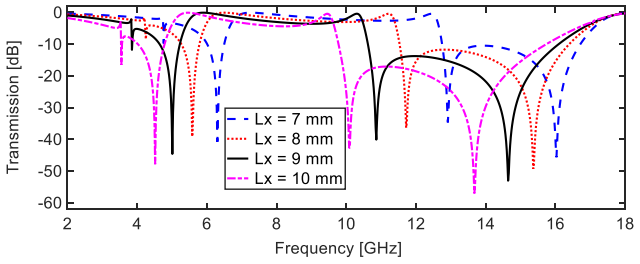

FIGURE 5. Simulated TC of the proposed multi-band LCPC for different *Lx*-parameter in terms of txx.

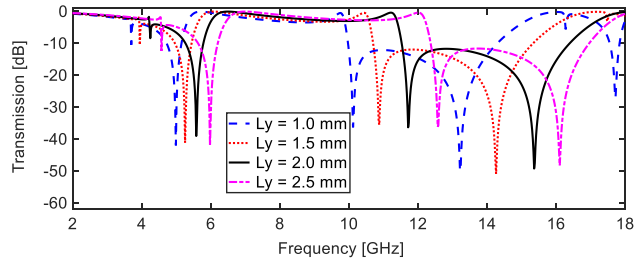

FIGURE 6. Simulated TC of the proposed LCPC for different *Ly*-parameter in terms of txx.

VII. ANGULAR STABILITY

In practice, the angle of the incident wave experienced by the LCPC surface is not always constant. Different factors such as weather conditions and the type of radiation antenna can cause fluctuations in the incident wave angle. Therefore, it is necessary to investigate the response of the LCPC to EM waves with different radiation angles. In this section, we examine the stability of LCPC performance when subjected to changes in the input EM wave radiation angle while keeping other parameters constant.

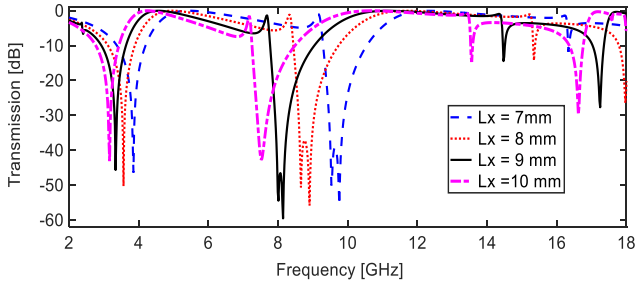

FIGURE 7. Simulated TC of the proposed LCPC for different *Lx*-parameter in terms of tyy.

for the *Lx* and *Ly*- parameters were set to 7mm and 2mm, respectively. There is an increase (reduction) in capacitive characteristics when the *Lx*-parameter (*Ly*-parameter) length is increased. Consequently, the corresponding impedance associated with $Z = 1/j\omega C$ decreases (increases), as seen in Fig. 5 through Fig.8. Following the equation $f = 1/\sqrt{LC}$, the resonant frequency shifts downward (upward).

As illustrated in Fig. 9 and Fig.10, the magnitude of the copolarized TCs, namely txx and tyy, remains nearly constant as the incident wave angle expands to approximately 50°. The simulated characteristics of the AR for incident angle from 0° to 50° are presented in Fig.11. The AR remains below 3dB for any increase in the radiation angle up to approximately 50° across all operating bands. Minor variations in the axial

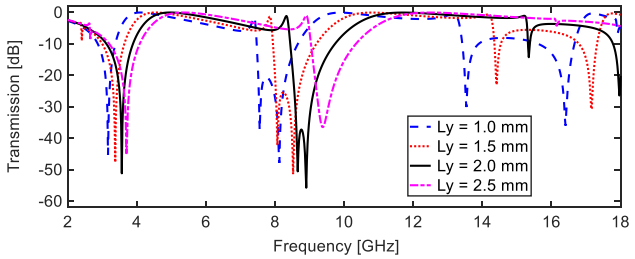

FIGURE 8. Simulated TC of the proposed LCPC for different *Ly*-parameter in terms of tyy.

ratio bandwidth (ARBW) of the LCPC are observed when altering the radiation angle from 0° to 50°. It should be noted that achieving angular stability in the converter relies on the precise design of the vias as part of the SIW structure. More over SIW technology is expected to overcome the challenges associated with polarization conversion due to its high-quality factor and high-power handling capability. Consequently, SIW technology is utilized to improve polarization conversion efficiency [38]. Furthermore, using the SIW technique creates electric currents perpendicular to the structure of the converter and increases the concentration of electric fields inside the area surrounded by the vias in this work. This phenomenon increases the transmission efficiency [39].

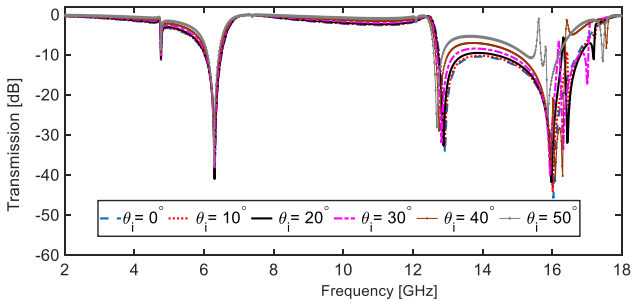

FIGURE 9. Simulated TC of the proposed LCPC for different incident angles in terms of txx.

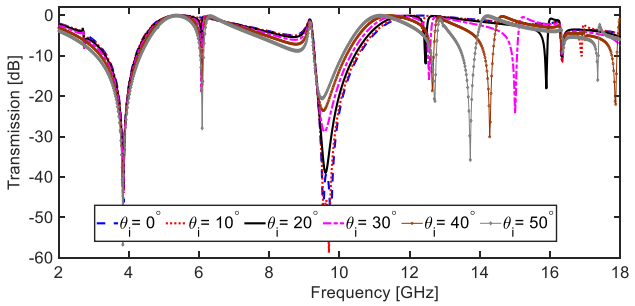

FIGURE 10. Simulated TC of the proposed LCPC for different incident angles in terms of tyy.

VIII. EQUIVALENT CIRCUIT MODEL

To elucidate the operational principles of the LCPC, we employed the advanced design system (ADS) software

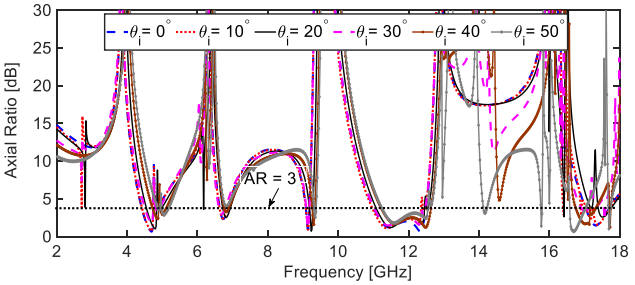

FIGURE 11. Simulated AR of the proposed LCPC for different incident angles.

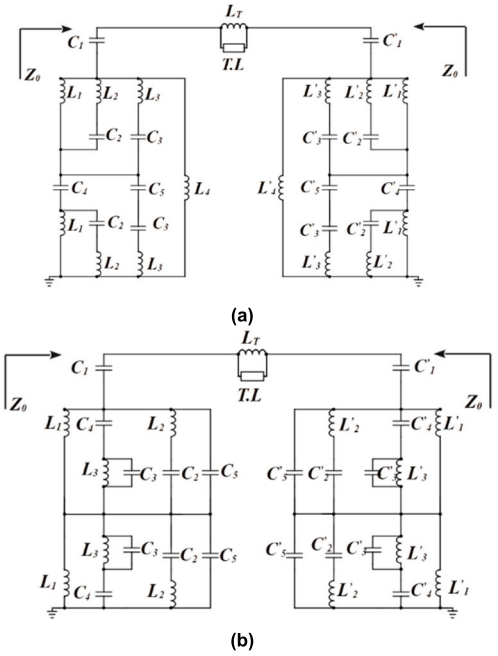

FIGURE 12. Equivalent circuit of the proposed LCPC under (a) y- polarized incident wave, (b) x- polarized incident wave.

to derive the equivalent circuit model (ECM) for both under *y*- and *x*-direction incident wave. Figure 12 illustrates the ECMs, where the inductors have been substituted with metallic components in the UC pattern, and capacitors emulate the intervening gap. In both orthogonal models, the inductor LT represents the via, while the capacitor signifies the capacitance between the vias and the designated structure. In *y*-polarized condition, a parallel amalgamation of inductors and capacitors models the UC curves, with the inductor representing the strip positioned in the UC's center. In the *x*-polarized mode, the capacitor models the horizontal arm. The specific values of the equivalent circuit elements are outlined in Table 2. After the equalization process, we compared the extracted TC of the ECM with those of the simulated LCPC UC, as illustrated in Fig. 13. It is imperative to highlight that while the CST software encompasses all coupling effects, the ADS software solely incorporates the floquet mode, resulting in disparities between the obtained results.

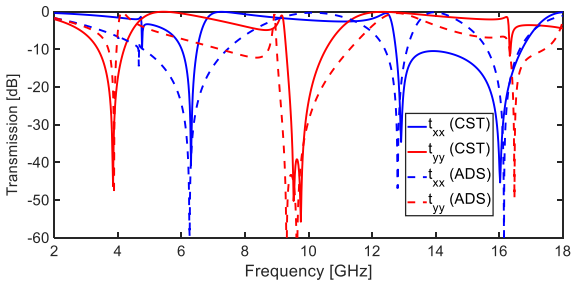

FIGURE 13. Simulated (by CST) and equivalent circuit modelling (by ADS) of Co-polarized TC of the proposed multi-band LCPC.

TABLE 2. Values of the equivalent circuit elements.

Incident Wave	Inductance	(nH)	Capacitance	(pF)
y- polarized	L_1	1.37	C_1	1.2
	L_2	1.51	C_2	0.089
	L_3	1.01	C_3	1.73
	L_4	4.93	C_4	0.11
	L_1'	1.28	C_5	2.6
	L_2'	1.97	C_1'	0.99
	L_3'	1.10	C_2'	0.8
	L_4'	3.90	C_3'	2.3
	L_T	17.80	C_4'	0.19
	--	--	C_5'	1.6
x- polarized	L_1	0.01	C_1	0.12
	L_2	0.80	C_2	0.11
	L_3	7.3	C_3	0.50
	L_1'	1.01	C_4	0.01
	L_2'	1.97	C_5	0.012
	L_3'	6.7	C_1'	0.11
	L_T	23	C_2'	0.01
	--	--	C_3'	0.32
	--	--	C_4'	0.06
	--	--	C_5'	0.10

IX. LABORATORY PROCEDURES AND RELATED RESULTS

Figure.14 presents the LCPC prototypes, including both simulated and fabricated samples, along with their corresponding measurement setups. The proposed LCPC, which is based on a single substrate, is fabricated using the conventional printed circuit board (PCB) process. The LCPC samples feature a 16×16 UC configuration and have dimensions of 192 mm × 192 mm. For the purpose of measurement, two LP horn antennas are employed, covering the frequency range of 1-18 GHz. These antennas are connected to a vector network analyzer (VNA) through coaxial cables. During the measurement process, one of the LP horn antennas functions as the transmitting antenna, while the other serves as the receiving antenna. The LCPC sample is positioned between the aforementioned LP horn antennas, with absorber materials employed to mitigate the influence of diffracted waves on the measurement process.

The distance between two standard horn antennas is a critical factor in measuring the S-parameters. Different factors must be considered to determine the appropriate distance,

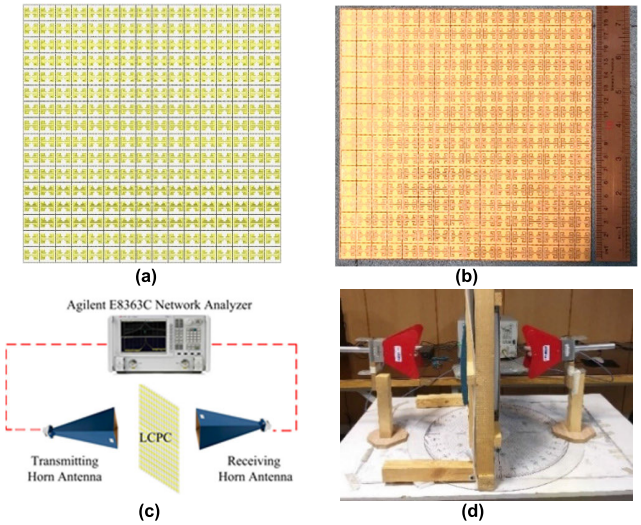

FIGURE 14. A 16 × 16 square array of the LCPC UC (a) Schematic of the proposed LCPC, (b) Fabricated prototype of the proposed LCPC, (c) Diagram of the measurement setup and (d) Experimental setup.

including the operation frequency, the size of the antennas, and the desired measurement accuracy. The distance should be selected so that the EM fields are well-developed and represent conditions in the far-field. It is recommended that the distance be sufficient to allow the fields to fully develop and form a plane wave before reaching the receiving antenna. As a general rule, the receiving antenna should be placed at a distance from the transmitting antenna that comes within the radius of the far-field region (also known as the Fraunhofer distance [40]). The Fraunhofer distance can be approximated using the flowing equation:

$$L = 2D^2/\lambda \tag{13}$$

where: D is the maximum dimension of the antenna aperture, λ is the wavelength of the highest operating frequency, and L is the Fraunhofer distance. To ensure accurate far-field measurements, the distance between standard horn antennas should be greater than the Fraunhofer distance. In this work, the maximum dimension of the standard horn antenna aperture is 175 mm, and the highest operating frequency is $f_{35} = 17.33$ GHz. Therefore, based on (13), the L becomes about 350 cm. Accordingly the appropriate distance should be greater than 350 cm, set at 400 cm, to ensure the far-field conditions in the antenna laboratory. On the other hand, regarding the distance between the LCPC surface and the transmitting antenna, considering that one of the main advantages of the transmissive-type LCPC is that the LCPC surface can be substantially closer to the antenna in comparison with reflective-type [17], we considered the distance between the transmitting antenna and the LCPC to be 10 cm. In addition, the optimal value of the distance can be obtained by studying the gain and axial ratio versus the frequency for different distance values [28]. The TCs are displayed by the VNA. To compute the AR, (9) is utilized, whereby the experimental

TABLE 3. Performance comparison among LCPCs.

Ref	Center Freq (GHz)	3-dB ARBW	Thickness	Cell Size	Number of Metallic Layers	Angular Stability
26	7.6, 13	31%, 13.8%	$0.24\lambda_0$	$0.22\lambda_0 \times 0.23\lambda_0$	4	25°
28	20, 29.8	2.5%, 1.7%	$0.07\lambda_0$	$0.35\lambda_0$	3	30°
30	19.6, 29.6	4%, 2.7%	$0.31\lambda_0$	--	5	--
38	8.8, 10.3	--	$0.02\lambda_0$	$0.10\lambda_0$	2	--
39	9.8, 11.8	--	$0.03\lambda_0$	$0.21\lambda_0$	2	--
40	15.1, 16.5	11.8%, 6.9%	$0.04\lambda_0$	$0.40\lambda_0$	2	--
41	18.5, 29	29%, 12%	$0.1\lambda_0$	$0.25\lambda_0$	2	20°
This work	4.65, 6.65, 9.10,11.65, 17.33	8.2%, 4.4%,2.9%, 12.87%, 3.2%	$0.024\lambda_0$	$0.18\lambda_0 \times 0.18\lambda_0$	1	50°

Angular Stability = highest incidence angle with 3-dB ARBW vary within 4% and λ_0 = free-space wavelength at lower band center.

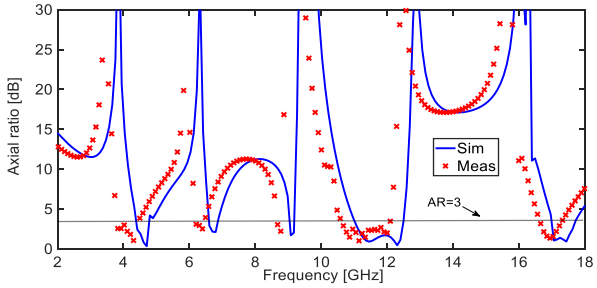

FIGURE 15. Simulated and measured AR of the proposed LCPC.

determination of the magnitude and phase difference of the TCs for x- and y-polarized EM waves is employed. The graphical representation of the AR criterion is depicted in Fig.15.

The results indicate that the minimum AR values measured across the five operating frequency bands of the LCPC, ordered from the lowest to the highest frequency band, were 1.05 dB, 2.2 dB, 1.9 dB, 1.01 dB, and 1.35 dB. The current investigation presents the findings of the measured 3-dB ARBW in five discrete frequency ranges: 3.9-4.43 GHz, 6.21-6.52 GHz, 8.9-9.08 GHz, 10.51-11.78 GHz, and 16.85-17.39 GHz. The approximate ARBW values for these ranges are 12.72%, 4.8%, 2.4%, 11.39%, and 3.15%, respectively. A notable observation is the strong agreement between the experimental and simulated AR results, as depicted in Fig.15. However, a slight disparity between the measured and simulated at outcomes may be attributed to factors such as manufacturing inaccuracies or the influence of the measurement environment on the results. The simulation and measurement procedures employed the CST software and the Agilent E8363C VNA, respectively. By leveraging a single-layered LCPC design, the proposed approach surpasses previous works regarding operational bands number, reduced thickness, compact cell dimensions, and enhanced stability at different incident angles. For a comprehensive performance comparison, refer to Table 3. It should be noted that in this work, 4% tolerance in angular stability is included due to the possibility of error in construction, testing, simulation and calculations.

X. CONCLUSION

The LCPC design proposed in this study is implemented on a Rogers 4003 substrate and follows a three-step fabrication process. The dimensions of the UC are specified as 12 mm × 12 mm × 1.57 mm. Experimental results substantiate the LCPC's capability to convert LP waves into CP waves across five distinct frequency bands. The proposed LCPC offers notable advancements over existing prototypes. Firstly, it distinguishes itself by providing practical utilization in five frequency bands. Secondly, it is constructed on a single-layer substrate, contributing to simplified fabrication procedures and yielding a lightweight and thin structure. Thirdly, it demonstrates cost-effectiveness. Fourthly, it exhibits stable performance over a wide angular range of ±50°. Lastly, the output waveform manifests RHCP properties in the first and fourth bands, while the remaining operating bands exhibit LHCP characteristics. Measurements conducted validate the effectiveness and suitability of the proposed LCPC structure, particularly for telecommunications applications involving the conversion of LP waves to CP waves in the C-, X-, and Ku-bands. Notably, the C- and Ku-bands are specifically designated for satellite transmissions, whereas X-band frequencies commonly find usage in naval, government, and defense applications.

ACKNOWLEDGMENT

The authors would like to thank the Northwest Antenna and Microwave Research Laboratory (NAMRL), Urmia University for their valuable assistance in the construction and testing of LCPC.

REFERENCES

[1] A. Eslami, J. Nourinia, C. Ghobadi, and M. Shokri, "Four-element MIMO antenna for X-band applications," *Int. J. Microw. Wireless Technol.*, vol. 13, no. 8, pp. 859–866, Jan. 2021, doi: 10.1017/s1759078720001440.

[2] A. Siahcheshm, J. Nourinia, C. Ghobadi, and M. Shokri, "Circularly polarized printed helix antenna for L- and S-bands applications," *Radioengineering*, vol. 29, no. 1, pp. 67–73, Apr. 2020, doi: 10.13164/re.2020.0067.

[3] S. Mohammadi, J. Nourinia, C. Ghobadi, J. Pourahmadazar, and M. Shokri, "Compact broadband circularly polarized slot antenna using two linked elliptical slots for C-band applications," *IEEE Antennas Wireless Propag. Lett.*, vol. 12, pp. 1094–1097, 2013, doi: 10.1109/LAWP.2013.2280457.

[4] H. Oraizi and S. Hedayati, "Miniaturization of microstrip antennas by the novel application of the Giuseppe Peano fractal geometries," *IEEE Trans. Antennas Propag.*, vol. 60, no. 8, pp. 3559–3567, Aug. 2012, doi: 10.1109/TAP.2012.2201070.

[5] J. Wu and K. Sarabandi, "Compact omnidirectional circularly polarized antenna," *IEEE Trans. Antennas Propag.*, vol. 65, no. 4, pp. 1550–1557, Apr. 2017, doi: 10.1109/TAP.2017.2669959.

[6] G. Zheng and B. Sun, "High-gain normal-mode omnidirectional circularly polarized antenna," *IEEE Antennas Wireless Propag. Lett.*, vol. 17, no. 6, pp. 1104–1108, Jun. 2018, doi: 10.1109/LAWP.2018.2834477.

[7] M. Fartookzadeh and S. H. Mohseni Armaki, "Circular feeding network for circular polarisation reconfigurable antennas," *Electron. Lett.*, vol. 55, no. 12, pp. 677–679, Jun. 2019, doi: 10.1049/el.2019.0920.

[8] Y. F. Lin, H. M. Chen, C. H. Chen, and C. H. Lee, "Compact shorted inverted-L antenna with circular polarisation for RFID handheld reader," *Electron. Lett.*, vol. 49, no. 7, pp. 442–444, Mar. 2013, doi: 10.1049/el.2012.4296.

[9] Q. Liu, Y. Liu, Y. Wu, M. Su, and J. Shen, "Compact wideband circularly polarized patch antenna for CNSS applications," *IEEE Antennas Wireless Propag. Lett.*, vol. 12, pp. 1280–1283, 2013, doi: 10.1109/LAWP.2013.2283218.

[10] H. W. Lai, K. M. Mak, and K. F. Chan, "Novel aperture-coupled microstrip-line feed for circularly polarized patch antenna," *Prog. Electromagn. Res.*, vol. 144, pp. 1–9, 2014, doi: 10.2528/pier13101803.

[11] B. A. Munk, *Frequency Selective Surfaces*. Hoboken, NJ, USA: Wiley, 2005.

[12] M. Akbari, S. Gupta, M. Farahani, A. R. Sebak, and T. A. Denidni, "Gain enhancement of circularly polarized dielectric resonator antenna based on FSS superstrate for MMW applications," *IEEE Trans. Antennas Propag.*, vol. 64, no. 12, pp. 5542–5546, Dec. 2016, doi: 10.1109/TAP.2016.2623655.

[13] H. Li, B.-Z. Wang, G. Zheng, W. Shao, and L. Guo, "A reflectarray antenna backed on FSS for low RCS and high radiation performances," *Prog. Electromagn. Res. C*, vol. 15, pp. 145–155, 2010, doi: 10.2528/pierc10070303.

[14] E. Doumanis, G. Goussetis, J. L. Gomez-Tornero, R. Cahill, and V. Fusco, "Anisotropic impedance surfaces for linear to circular polarization conversion," *IEEE Trans. Antennas Propag.*, vol. 60, no. 1, pp. 212–219, Jan. 2012, doi: 10.1109/TAP.2011.2167920.

[15] M. Fartookzadeh and S. H. Mohseni Armaki, "Dual-band reflection-type circular polarizers based on anisotropic impedance surfaces," *IEEE Trans. Antennas Propag.*, vol. 64, no. 2, pp. 826–830, Feb. 2016, doi: 10.1109/TAP.2015.2511152.

[16] S. Ghosh, J. Ghosh, M. Santoshkumar Singh, and A. Sarkhel, "A low-profile multifunctional metasurface reflector for multiband polarization transformation," *IEEE Trans. Circuits Syst. II, Exp. Briefs*, vol. 70, no. 1, pp. 76–80, Jan. 2023, doi: 10.1109/TCSII.2022.3202085.

[17] F. Zhang, G.-M. Yang, and Y.-Q. Jin, "Design and analysis of linear to circular polarization converter with third-order meta-frequency selective surfaces," *IEEE Trans. Antennas Propag.*, vol. 68, no. 9, pp. 6646–6655, Sep. 2020, doi: 10.1109/TAP.2020.2982503.

[18] P. Fei, Z. Shen, X. Wen, and F. Nian, "A single-layer circular polarizer based on hybrid meander line and loop configuration," *IEEE Trans. Antennas Propag.*, vol. 63, no. 10, pp. 4609–4614, Oct. 2015, doi: 10.1109/TAP.2015.2462128.

[19] M.-A. Joyal and J.-J. Laurin, "Analysis and design of thin circular polarizers based on meander lines," *IEEE Trans. Antennas Propag.*, vol. 60, no. 6, pp. 3007–3011, Jun. 2012, doi: 10.1109/TAP.2012.2194659.

[20] S. M. A. Momeni Hasan Abadi and N. Behdad, "Wideband linear-to-circular polarization converters based on miniaturized-element frequency selective surfaces," *IEEE Trans. Antennas Propag.*, vol. 64, no. 2, pp. 525–534, Feb. 2016, doi: 10.1109/TAP.2015.2504999.

[21] W. Zhang, J.-Y. Li, and J. Xie, "A broadband circular polarizer based on cross-shaped composite frequency selective surfaces," *IEEE Trans. Antennas Propag.*, vol. 65, no. 10, pp. 5623–5627, Oct. 2017, doi: 10.1109/TAP.2017.2735459.

[22] Y. Ranga, L. Matekovits, S. G. Hay, and T. S. Bird, "An anisotropic impedance surface for dual-band linear-to-circular transmission polarization convertor," in *Proc. Int. Workshop Antenna Technol. (iWAT)*, Mar. 2013, pp. 47–50, doi: 10.1109/IWAT.2013.6518296.

[23] C. Pfeiffer and A. Grbic, "Millimeter-wave transmitarrays for wavefront and polarization control," *IEEE Trans. Microw. Theory Techn.*, vol. 61, no. 12, pp. 4407–4417, Dec. 2013, doi: 10.1109/TMTT.2013.2287173.

[24] M. Mutlu, A. E. Akosman, A. E. Serebryannikov, and E. Ozbay, "Asymmetric chiral metamaterial circular polarizer based on four U-shaped split ring resonators," *Opt. Lett.*, vol. 36, no. 9, p. 1653, May 2011, doi: 10.1364/ol.36.001653.

[25] S.-Y. Wang, W. Liu, and W. Geyi, "Dual-band transmission polarization converter based on planar-dipole pair frequency selective surface," *Sci. Rep.*, vol. 8, no. 1, pp. 1–9, Feb. 2018, doi: 10.1038/s41598-018-22092-4.

[26] Q. Zeng, W. Ren, H. Zhao, Z. Xue, and W. Li, "Dual-band transmission-type circular polariser based on frequency selective surfaces," *IET Microw., Antennas Propag.*, vol. 13, no. 2, pp. 216–222, Feb. 2019, doi: 10.1049/iet-map.2018.5613.

[27] P. Naseri, C. A. Fernandes, S. A. Matos, and J. R. Costa, "Antenna-filter-antenna-based cell for linear-to-circular polarizer transmit-array," in *Proc. IEEE Int. Symp. Antennas Propag. USNC/URSI Nat. Radio Sci. Meeting*, Jul. 2017, pp. 1071–1072, doi: 10.1109/APUSNCURSINRSM.2017.8072578.

[28] P. Naseri, S. A. Matos, J. R. Costa, C. A. Fernandes, and N. J. G. Fonseca, "Dual-band dual-linear-to-circular polarization converter in transmission mode application to *K*/*Ka*-band satellite communications," *IEEE Trans. Antennas Propag.*, vol. 66, no. 12, pp. 7128–7137, Dec. 2018, doi: 10.1109/TAP.2018.2874680.

[29] A. Abbaspour-Tamijani, K. Sarabandi, and G. M. Rebeiz, "Antenna–filter–antenna arrays as a class of bandpass frequency-selective surfaces," *IEEE Trans. Microw. Theory Techn.*, vol. 52, no. 8, pp. 1781–1789, Aug. 2004, doi: 10.1109/TMTT.2004.831572.

[30] M. Hosseini and S. V. Hum, "A systematic circuit-based approach to efficiently realize singleand dual-band circular polarizers," in *Proc. 12th Eur. Conf. Antennas Propag. (EuCAP)*, Apr. 2018, vol. 1, no. 5, pp. 98–103, doi: 10.1049/cp.2018.0734.

[31] Y. Youn and W. Hong, "Planar dual-band linear to circular polarization converter using radial-shape multi-layer FSS," in *Proc. IEEE Int. Symp. Antennas Propag. USNC/URSI Nat. Radio Sci. Meeting*, Jul. 2018, pp. 1465–1466, doi: 10.1109/apusncursinrsm.2018.8608738.

[32] S. Khan and T. F. Eibert, "A dual-band metasheet for asymmetric microwave transmission with polarization conversion," *IEEE Access*, vol. 7, pp. 98045–98052, 2019, doi: 10.1109/ACCESS.2019.2929115.

[33] A. K. Fahad, C. Ruan, S. A. K. M. Ali, R. Nazir, T. U. Haq, S. Ullah, and W. He, "Triple-wide-band ultra-thin metasheet for transmission polarization conversion," *Sci. Rep.*, vol. 10, no. 1, pp. 1–12, Jun. 2020, doi: 10.1038/s41598-020-65881-6.

[34] L. Yuan, L. Hou, Z. Yang, and Z. Zhang, "Triple-band ultra-thin linear to circular polarization converter based on transmission metasurface," *Microw. Opt. Technol. Lett.*, vol. 64, no. 1, pp. 54–59, Sep. 2021, doi: 10.1002/mop.33042.

[35] M. A. Sofi, K. Saurav, and S. K. Koul, "Frequency-selective surface-based compact single substrate layer dual-band transmission-type linear-to-circular polarization converter," *IEEE Trans. Microw. Theory Techn.*, vol. 68, no. 10, pp. 4138–4149, Oct. 2020, doi: 10.1109/TMTT.2020.3002248.

[36] L. Di Palma, A. Clemente, L. Dussopt, R. Sauleau, P. Potier, and P. Pouliguen, "Circularly polarized transmitarray with sequential rotation in Ka-band," *IEEE Trans. Antennas Propag.*, vol. 63, no. 11, pp. 5118–5124, Nov. 2015, doi: 10.1109/TAP.2015.2474149.

[37] H. Shirzad, C. Ghobadi, and J. Nourinia, "Circularly polarized dual-band dipole antenna utilizing a transmissive type linear to circular polarization converter," *AEU-Int. J. Electron. Commun.*, vol. 166, Jul. 2023, Art. no. 154649, doi: 10.1016/j.aeue.2023.154649.

[38] H. Chen, L. Han, R. Zhao, F. Li, Y. Zhou, Z. Zhou, X. Li, X. Weng, D. Liang, J. Xie, and L. Deng, "Design of the high-efficiency transmission-type polarization converter based on substrate-integrated waveguide (SIW) technology," *Appl. Phys. A, Solids Surf.*, vol. 125, no. 4, pp. 1–7, Mar. 2019, doi: 10.1007/s00339-019-2555-3.

[39] M. S. M. Mollaei, "Narrowband configurable polarization rotator using frequency selective surface based on circular substrate-integrated waveguide cavity," *IEEE Antennas Wireless Propag. Lett.*, vol. 16, pp. 1923–1926, 2017, doi: 10.1109/LAWP.2017.2688703.

[40] R. W. Bickmore, "Fraunhofer pattern measurement in the Fresnel region," *Can. J. Phys.*, vol. 35, no. 11, pp. 1299–1308, Nov. 1957, doi: 10.1139/p57-142.

HAMED SHIRZAD was born in Urmia, Iran, in 1985. He received the B.Sc. degree in electrical and communication engineering from IAU, Urmia, in 2008, and the M.Sc. degree in electrical and communication engineering from Urmia University, in 2011, where he is currently pursuing the Ph.D. degree in communication engineering with the Department of Electrical Engineering. He has published more than ten scientific articles in multiple journals with the cooperation of the Northwest Antenna and Microwave Research Laboratory (NAMRL), Urmia University. His research interests include microstrip antennas, fractal antennas, and polarizers.

CHANGIZ GHOBADI received the B.Sc. degree in electrical engineering and the M.Sc. degree in electrical engineering telecommunication from the Isfahan University of Technology, Isfahan, Iran, and the Ph.D. degree in electrical telecommunication from the University of Bath, Bath, U.K., in 1998. He is currently a Professor with the Department of Electrical Engineering, Urmia University, Urmia, Iran. He has supervised and administered more than 130 M.Sc. and 32 Ph.D. students and their thesis. He has authored or coauthored more than 360 scientific publications including accredited journals and conferences. His articles have been cited more than 5750 times. He has been included in the Top One Percent of the World's Scientists and Academics according to Thomson Reuters' list, in 2017, 2020, and 2022. His research interests include antenna design, radar, and adaptive filters.

JAVAD NOURINIA (Senior Member, IEEE) received the B.Sc. degree in electrical and electronic engineering from Shiraz University, the M.Sc. degree in electrical and telecommunication engineering from the Iran University of Science and Technology, and the Ph.D. degree in electrical and telecommunication from the University of Science and Technology, Tehran, Iran, in 2000. He was the Head of the Faculty Engineering Department, from 2013 to 2017, and a Distinguished Professor with Urmia University. He has been included in the Top One Percent of the World's Scientists and Academics according to Thomson Reuters' list, since 2016. His research interests include small antennas, filters, MIMO antennas, periodic structures, optimization, and measurement.

MAJID SHOKRI (Graduate Student Member, IEEE) received the Ph.D. degree in telecommunication engineering from Urmia University, Urmia, Iran, in 2023. Since 2018, he has been a Researcher with the Northwest Antenna and Microwave Research Laboratory (NAMRL), Urmia University. He has published more than 20 scientific articles in multiple journals and is a reviewer of respected journals. His research interests include microstrip antennas, circular polarization, BTS, and microwave circuits.

MOHSEN KARAMIRAD received the Ph.D. degree in electrical engineering from Urmia University, in 2020. He has been a Postdoctoral Researcher with Urmia University, since 2021. His research interests include antenna design and metasurfaces.